Materials Today Energy 21 (2021) 100743

Contents lists available at ScienceDirect

Materials Today Energy

journal homepage: www.journals.elsevier.com/materials-today-energy/

High-performance copper selenide thermoelectric thin films for flexible thermoelectric application

X.-L. Huang [a], D.-W. Ao [a], T.-B. Chen [a, b], Y.-X. Chen [a], F. Li [a], S. Chen [a], G.-X. Liang [a], X.-H. Zhang [b], Z.-H. Zheng [a, *], P. Fan [a]

[a] Shenzhen Key Laboratory of Advanced Thin Films and Applications, Key Laboratory of Optoelectronic Devices and Systems of Ministry of Education and Guangdong Province, College of Physics and Optoelectronic Engineering, Shenzhen University, Shenzhen, 518060, PR China
[b] Univ Rennes, CNRS, ISCR (Institut des Sciences Chimiques de Rennes) UMR6226, Rennes, F-35000, France

ARTICLE INFO

Article history:
Received 29 January 2021
Received in revised form
8 March 2021
Accepted 29 March 2021
Available online 7 April 2021

Keywords:
Thermoelectric materials
Thin film
Cu_2Se
Flexible

ABSTRACT

Flexible thermoelectric (TE) materials have wide applications in fabricating portable/wearable devices owing to the advantages of being bendable, small size, and lightweight. Inorganic material–based flexible thin films have attracted much attention owing to their high TE performance. So far, developing high TE properties and environment friendly flexible thin films for practical applications is still a considerable challenge. Copper selenide (Cu_2Se) is a non-toxic and low-cost material, providing relatively safe TE modules for thin film devices. In this work, Cu_{2Se}-based thin films with single crystal phase have been fabricated successfully at a flexible substrate by an efficient layer-by-layer combination reaction method. By optimizing the composition, a high power factor of 5.3 $\mu Wcm^{-1}K^{-2}$ and dimensionless figure of merit value of 0.35 with low thermal conductivity are achieved at room temperature. Through bending tests, it has been shown that the prepared thin films possess good flexibility and the designed flexible device displays stable output power, which demonstrates the potential of inorganic TE materials to be mountable on flexible/wearable substrates for energy harvesting and management devices.

1. Introduction

Thermoelectric (TE) conversion is a solid-state, secure, convenient, and environment friendly energy conversion technology allowing the direct conversion of heat into electricity and vice versa, which has broad applications in cooling, power generation, and waste heat recovery [1–4]. The TE performance of TE materials is evaluated by the dimensionless figure of merit (ZT), $ZT = S^2\sigma T\kappa^{-1}$, where S is the Seebeck coefficient, σ is the electrical conductivity, κ is the thermal conductivity, and T is the absolute temperature. Besides, $S^2\sigma$ is called as power factor (PF), which is used to estimate the electronic properties [5]. Recently, the explosive growth of portable and wearable microelectronics has stimulated the development of flexible TE materials promising for applications in wearable devices such as the self-powered generator from the temperature difference between the skin and the ambient environment [6]. Therefore, fabricating high-performance flexible TE materials has received great attention, and significant work has been reported in the recent years [7–12]. Owing to the high performance of inorganic materials, research on depositing inorganic materials on flexible substrates such as fibers, organics, and carbon nanotubes has been widely reported [13–17]. Until now, most of the flexible thin films and devices were fabricated based on the classic Te-based materials because of their excellent TE properties [18,19]. However, Te-based materials remain a significant challenge for large-scale commercialization owing to the presence of less earth-abundant, toxic, and costly elements. Thus, developing low-cost and non-toxic TE thin films with acceptable performance to substitute Te-based materials is highly desired.

Recently, transition metal selenium compound semiconductor materials [20–24], especially copper selenide (Cu_2Se) [25], have attracted great attention for thermoelectrics. Non-toxic Cu_2Se has excellent TE properties such that a relatively large ZT value of more than 2.0 has already been achieved [26], making it extremely promising as a potential alternative for the traditional Te-based materials. Thus, fabricating high-performance Cu_2Se thin films has also been widely studied, and various methods, including solution [27,28], electrodeposition [29], pulsed laser deposition [30],

* Corresponding author.
E-mail address: zhengzh@szu.edu.cn (Z.-H. Zheng).

https://doi.org/10.1016/j.mtener.2021.100743
2468-6069/

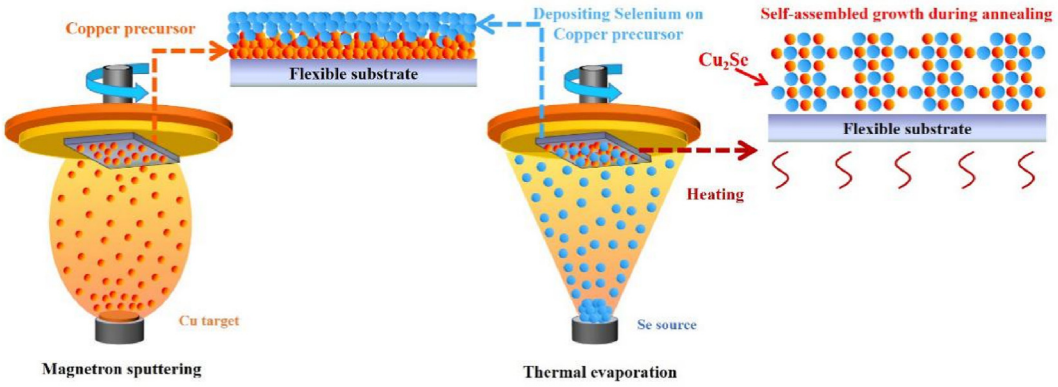

Fig. 1. The schematic diagram of fabricating the Cu2Se thin film. Cu2Se, copper selenide.

ion beam sputtering deposition [31], reactive evaporation [32], galvanic deposition [33], and pulsed/magnetron sputtering [34], have been used. For instance, Lin et al. [27] used the solution method to prepare Cu2Se-based thin film, resulting in a maximum PF of 4.6 $\mu Wcm^{-1}K^{-2}$ on the flexible polyimide substrate, respectively. Scimeca et al. optimized the carrier concentration of Cu_{2Se}-based thin films to significantly improve their TE properties through a soaking process in Cu^{+} ion solution [29]. However, the reported Cu_2Se thin films to date usually exhibit much lower TE properties than those of the bulk Cu_2Se.

Magnetron sputtering and thermal evaporation methods are commonly used to prepare thin films, especially for substances that are extremely susceptible to oxidation. Based on the advantages of these two technologies, it is expected to produce high-performance Cu_2Se thin films by using magnetron sputtering or the evaporation method. However, some unavoidable issues limit the use of these two technologies, i.e., Se has much high saturated vapor pressure and is not efficiently controllable during the sputtering process; Cu is difficult to evaporate because of its high boiling point. Therefore, there are only a few reports about Cu_2Se thin films prepared by magnetron sputtering or the evaporation method. In this work, an efficient layer-by-layer combination reaction method by integrating magnetron sputtering and thermal evaporation technology

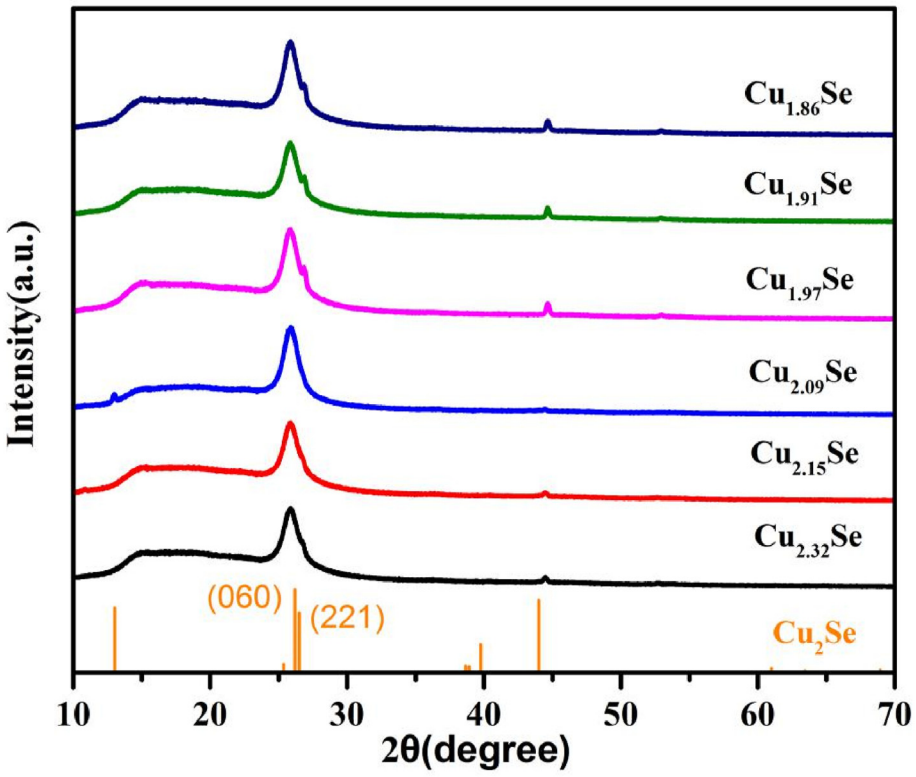

Fig. 2. XRD data of flexible Cu_2Se thin films with different composition ratios. XRD, X-ray diffraction; Cu2Se, copper selenide.

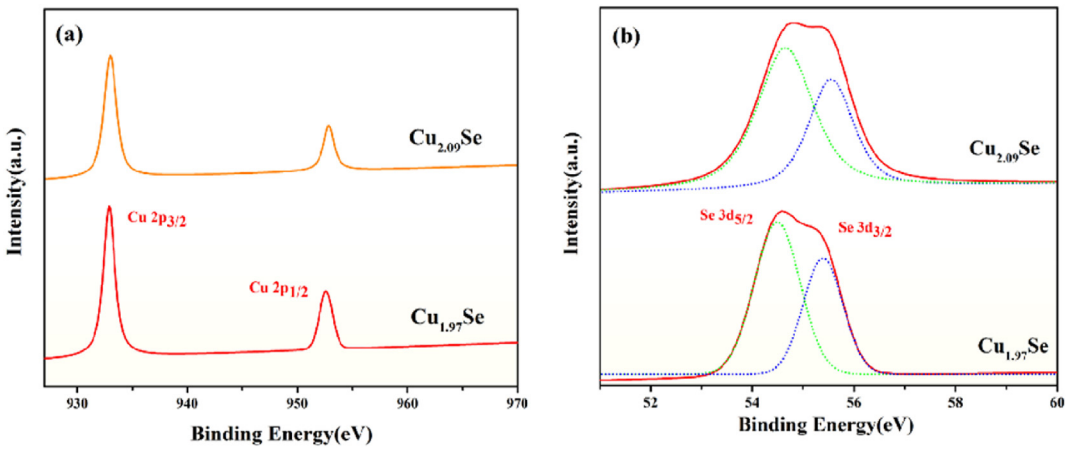

Fig. 3. XPS data of flexible Cu_2Se thin films at a composition ratio of the 1.97:1 and 2.09:1: (a) Cu and (b) Se. XPS, X-ray photoelectron spectroscopy; Cu2Se, copper selenide.

is developed to prepare flexible Cu_2Se thin films. The effect of composition content on the microstructure and TE properties of the flexible Cu_2Se thin films was systematically investigated.

2. Experimental section

The process of the Cu2Se-based thin film fabrication is represented by a schematic diagram in Fig. 1. At first, the Cu precursor layer was sputtered by using the magnetron sputtering deposition method, and the flexible Kapton polyimide film (200HN) are used as the substrate, which can be used at the temperatures up to 200 °C. The sputtering power, background pressure, and working pressure were maintained at 15 W, 8×10^{-4} Pa, and 1.6 Pa, respectively. The Cu layer is controlled to be 100 nm, with the sputtering rate of 1 $Å s^{-1}$. After completing Cu deposition, the Se layer was continued to deposit on the Cu precursor layer by using thermal evaporation deposition method at another deposition system. The working current of the evaporation source was 60 A, with the background pressure of 5.0×10^{-4} Pa. The average deposition rate of Se is ~0.8 $Å^{-1}$, which was controlled using a quartz microbalance, and the thickness of Se layer is varied from 70 nm to 120 nm. Finally, all the thin films with different Se contents were annealed at 200 °C for 1 h using a heating system in a glove box under nitrogen atmosphere.

Crystal structure of the thin films is analyzed by X-ray diffraction (XRD, Ultima-iv), with the 2θ angle ranging from 10° to 70°, using CuK_α radiation (under operation requirements of 40 mA and 40 kV). Surface topography of the Cu2Se-based thin film is investigated by scanning electron microscopy (SEM; Supra 55), with an electron beam accelerated at 5 kV. Composition is investigated by energy dispersive X-ray spectroscopy (EDS; Bruker Quantax 200) equipped with the SEM system. Transmission

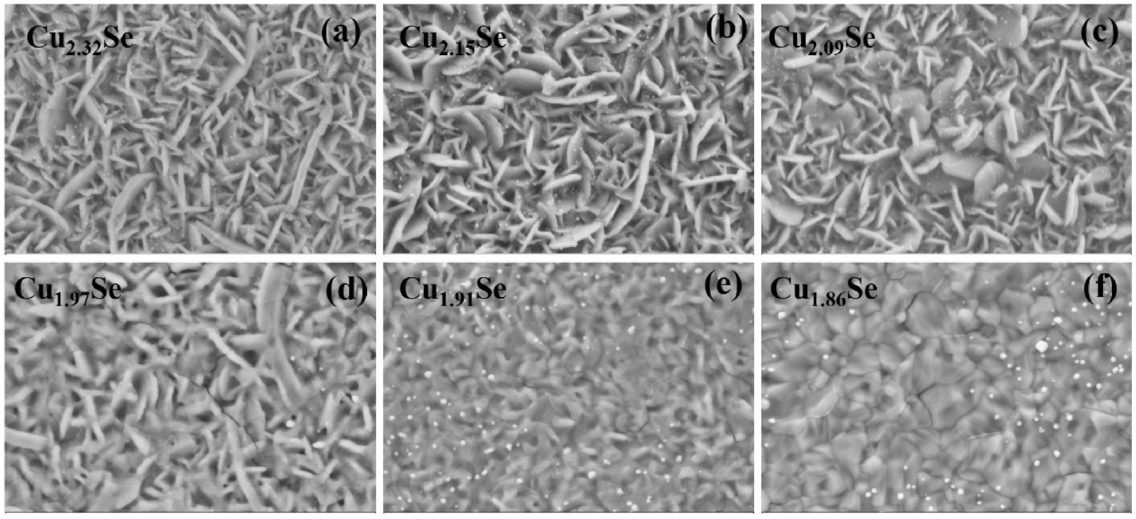

Fig. 4. SEM images of flexible Cu_2Se thin films at different composition ratios: (a) $Cu_{2.32}Se$, (b) $Cu_{2.15}Se$, (c) $Cu_{2.09}Se$, (d) $Cu_{1.97}Se$, (e) $Cu_{1.91}Se$, (f) $Cu_{1.86}Se$. SEM, scanning electron microscopy; Cu2Se, copper selenide.

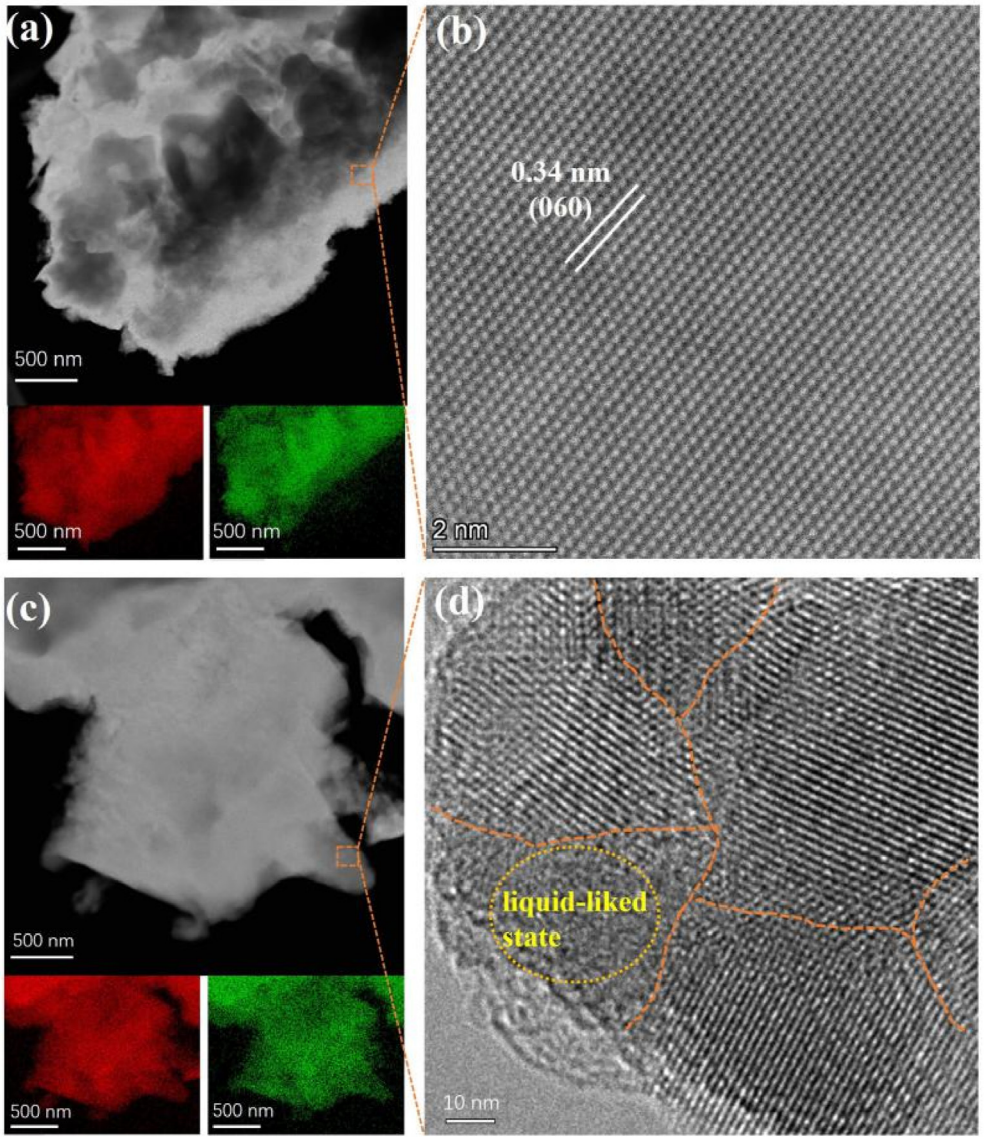

Fig. 5. (a) TEM characterization and EDS elemental mappings of the $Cu_{1.97}Se$ thin film. (b) Lattice fringes in (a) performed by HRTEM. (c) TEM characterization and EDS elemental mappings of the $Cu_{2.09}Se$ thin film. (d) Lattice fringes in (c) performed by HRTEM. HRTEM, high-resolution transmission electron microscopy; EDS, energy dispersive X-ray spectroscopy; TEM, transmission electron microscopy.

electron microscopy (TEM; JEM-3200FS) is used to measure the microstructure of the thin films. The chemical valence was characterized by conducting X-ray photoelectron spectroscopy (XPS; Escalab 250Xi) with a monochrome Al K_α X-ray source of 1486.6 eV. Before the test, the samples were plasma etched for 30 s to remove impurities on the surface of the thin film. The total thickness of the thin films was measured using a Dektak3 ST surface-profile measurement system and is shown in Table S1(Supporting information). The mobility and carrier density are investigated by van der Pauw-Hall measurement (HL5500PC, Nanometrics). In-plane electrical conductivity and Seebeck coefficient are measured using the Seebeck conductivity coefficient measurement system (SBA458, Netzsch). Thermal conductivity at room temperature is determined by a transient hot-wire theory method (TC3000, Xiatech). The current-voltage (I−V) curves of the TE device of thin films are measured using a Keithley 2400.

Table 1
Composition of the Cu-Se thin film as a function of Se layer thickness.

Se layer thickness (nm)	70	80	90	100	110	120
Cu (at.%)	69.9	68.3	67.6	66.3	65.6	65.0
Se (at.%)	30.1	31.7	32.4	33.7	34.4	35.0
Cu:Se	2.32:1	2.15:1	2.09:1	1.97:1	1.91:1	1.86:1

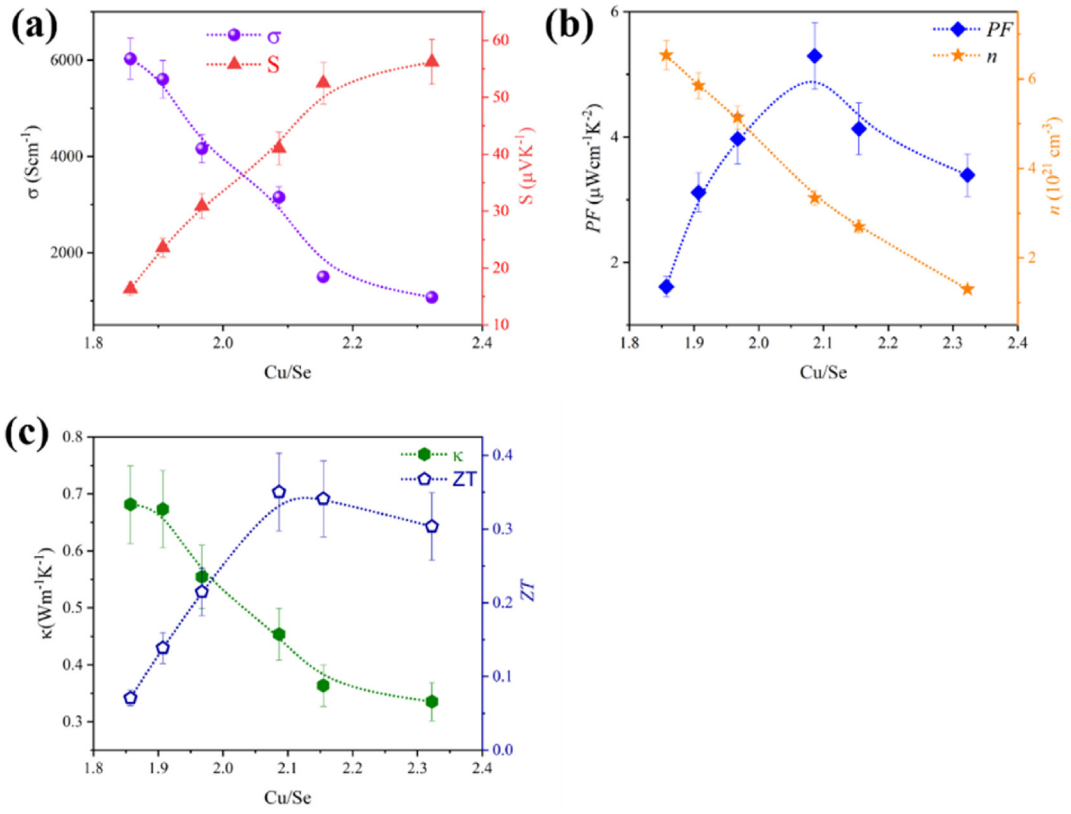

Fig. 6. The thermoelectric properties of flexible Cu_2Se thin films as function of atomic ratios: (a) electrical conductivity and Seebeck coefficient, (b) power factor and carrier concentration, and (c) thermal conductivity and *ZT*. ZT, dimensionless figure of merit; Cu2Se, copper selenide.

3. Results and analysis

The composition of the Cu-Se thin films was analyzed by EDS, as shown in Table 1. The Cu:Se atomic ratio is close to 2:1 when the Se layer thickness is 100 nm and show slightly Cu-excess and Se-excess when the Se thickness is less than and higher than 100 nm, respectively. For better discussion, the prepared Cu-Se thin films are named as $Cu_{2.32}Se$, $Cu_{2.15}Se$, $Cu_{2.09}Se$, $Cu_{1.97}Se$, $Cu_{1.91}Se$, and $Cu_{1.86}Se$, corresponding to the Cu atomic ratio in the thin films. Fig. 2 shows the phase structure of the thin films with different Cu contents measured by XRD. After comparing with the XRD pattern (PDF#37−1187) of the Cu2Se powder, it confirms that all the diffraction peaks of the samples belong to the cubic structure of Cu_2Se without impurity peaks, suggesting that the samples have good crystallinity with a single Cu_2Se phase. Moreover, as per the Debye Scherrer equation [35], the estimated grain size of the thin films (Fig. S1, Supporting information) calculated using the XRD data is around 25 nm, indicating the nanocrystallinity of the samples. The binding states of Cu and Se in the $Cu_{2.09}Se$ and $Cu_{1.97}Se$ samples are investigated by XPS. As shown in Fig. 3(a), the core level spectrum of the $Cu_{2.09}Se$ sample reveals that two strong peaks are obtained at ~933 eV of Cu $2p_{3/2}$ and ~953 eV of Cu $2p_{1/2}$, which are well matched with the spin-orbit phenomena of the compound state of Cu (I). A similar observation for Cu of the $Cu_{1.97}Se$ sample is obtained. Thus, the results suggest that both the Cu-excess and Cu-deficiency samples have a stable Cu^{1+} state [36]. A broad peak ranging from 53 to 57 eV is observed from the samples, as shown in Fig. 3(b). It can be identified that two symmetric peaks corresponding to Se $3d_{5/2}$ and Se $3d_{3/2}$, respectively, are located at 54.5 eV and 55.7 eV, which is the characteristic shape of compound Se (−II) in a consistent bonding environment [36]. In addition, no high-valence copper or selenium related to the oxidation state can be observed from the XPS patterns, which can be attributed to the fact that the thin film is prepared in vacuum and heat treatment is also carried in a low-oxygen environment. Combining the XRD and EDS results, it can be concluded that the prepared Cu_2Se thin films have few defects and good crystallinity, which is beneficial to obtain high TE performance.

The surface morphology of the samples is shown in Fig. 4. Nanosheet-like particles are observed on the surface of the Cu-excess samples, as shown in Fig. 4 (a), (b), and (c), indicating the flake structure of the thin films. The length of the nanoparticles decreases with the decrease in Cu content, whereas the width increases. Interestingly, compact particles without an obvious shape structure are obtained from the $Cu_{1.91}Se$ and $Cu_{1.86}Se$ samples. As shown in the XRD

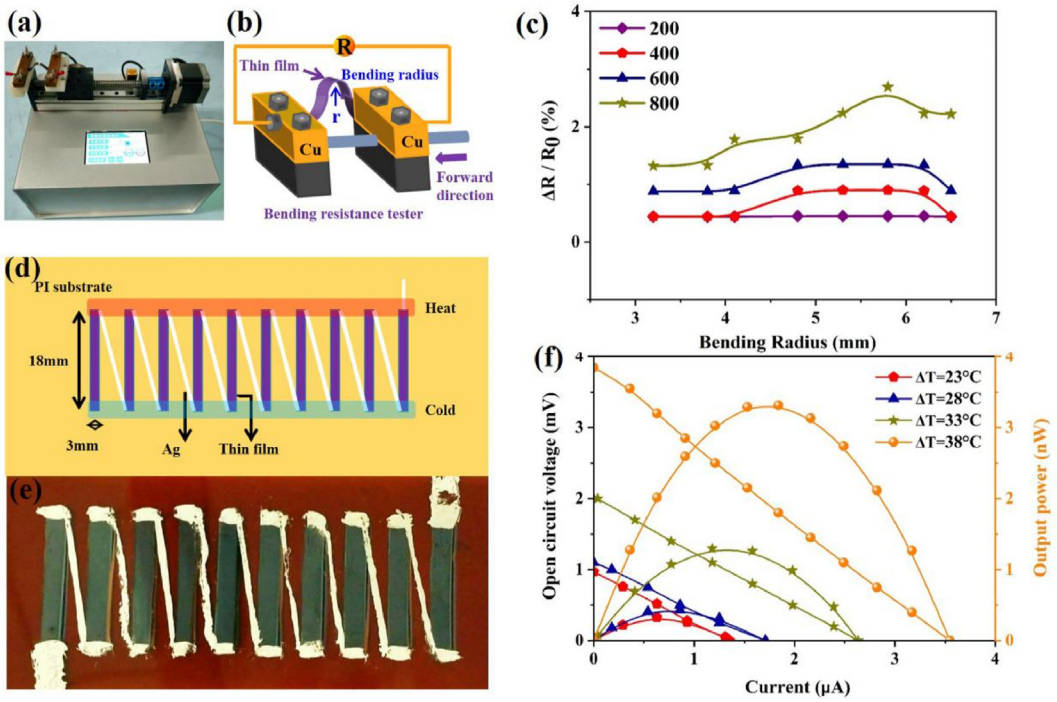

Fig. 7. The (a) optical image and (b) schematic diagram of the bending system. (c) The influence of bending cycle and bending radius on the resistance difference of the $Cu_{2.09}Se$ thin film. The (d) structure diagram and (e) optical image of the fabricated device. (f) Open voltage and output power as a function of current of the device.

results, the peak intensity increases and some addition peaks are observed after change in the composition ratio, indicating the change in the thin film growth structure. Thus, such difference in morphology is anticipated owing to the different stacked growth of the grains at different composition ratios. High-resolution TEM analysis of the sample is performed to further investigate the microstructure of the thin films. Fig. 5(a) displays the EDS mapping images of the $Cu_{1.97}Se$ sample and indicates that Cu and Se have uniform distribution. Fig. 5(b) shows the high-resolution TEM image and the measured lattice spacing is 3.42 Å, which correspond to the (060) plane of Cu_2Se. The $Cu_{2.09}Se$ sample also displays uniform distribution of Cu and Se, as shown in Fig. 5(c). Fig. 5(d) displays that crystalline nanoparticles stack compactly with each other, and the measured lattice spacing is 3.42 Å, which correspond to the (060) plane of Cu_2Se, suggesting the good crystallinity of the sample. Interestingly, no Cu-related crystal clusters are observed from the mapping image, which is in agreement with the XPS and XRD results. In general case, the ex-excess Cu might as the liquid-liked state and exists in the crystal grain's [37] which can also be seen in Fig. 5(d).

The room-temperature electrical conductivity σ and Seebeck coefficient S are shown in Fig. 6(a). With the increase in Cu content, σ decreases, which is attributed to the decrease in carrier concentration, as shown in Fig. 6(b). Conversely, the mobility (Table S2, Supporting information) increases when the Cu content increases, which benefits in obtaining a high S coefficient, and the maximum value can be achieved up to a value higher than 55 μVK^{-1}. *PF* of the samples are calculated and shown in Fig. 6(b). It increases first, reaches to a maximum value of 5.3 $\mu Wcm^{-1}K^{-2}$ from the $Cu_{2.09}Se$ sample, and then decreases when the Cu content continues to rise. Nevertheless, the achieved maximum *PF value* can be compared with one of the highest values of flexible Cu_2Se thin films prepared by another method [38]. The in-plane thermal conductivity of samples is shown in Fig. 6(c) and displays the decreasing trend with the increase in Cu content. Interestingly, the Cu-excess samples have low thermal conductivity κ. Based on the microstructure results as mentioned previously, it can be attributed as the nanostructure of the thin films, that scatter the mid- and long-length phonons more efficiently. The estimated ZT in Fig. 6(c) demonstrates that the Cu-excess samples have higher values than that of the Se-excess samples owing to the higher S and lower κ value. The maximum ZT value of 0.35 is achieved from the $Cu_{2.09}Se$ sample, which is close to the highest value at room temperature of the bulk Cu_2Se materials [39–41], indicating the effectiveness of this innovative technique for preparing high-performance flexible Cu_2Se TE thin films.

The mechanical property of the flexible thin film is measured using a bending resistance system, the schematic diagram and optical image of which are shown in Fig. 7(a) and (b). The relative resistance change ($\Delta R/R_0=(R'-R_0)/R_0$) was applied to quantitatively investigate the mechanical stability of the thin films, where R_0, R', and ΔR are the original resistance, bending resistance, and difference between R' and R_0, respectively [42]. The influence of bending radius (3.2 mm, 3.8 mm, 4.1 mm, 4.8 mm, 5.3 mm, 5.8 mm, 6.2 mm, 6.5 mm) and the bending cycles (200, 400, 600, 800) on the $\Delta R/R_0$ of the flexible thin films is shown in Fig. 7(c). It can be seen that $\Delta R/R_0$ is slightly increased with the increase in bending radius and bending cycles. The maximum difference of $\Delta R/R_0$ is about 3% when the bending cycles increased to 800, with the radius of 6.5 mm, which is close to the value reported from the literature [43], suggesting that the thin film has good flexible properties.

To show the potential energy harvesting applications of the present copper selenide thin film in wearable electronic devices, a simple TE device is fabricated. The structure diagram and optical image of the fabricated device are shown in Fig. 7(d) and (e). The device consists of 10 pieces of the thin film, and all legs were connected in series by painting silver paste. Fig. 7(f) shows the *I–V* curves and current-power curves of the device at different temperature differences ($\Delta T = T_{hot} - T_{cold}$). As shown in Fig. 7(f), the open circuit voltage (U_{oc}) was 0.96 mV, 1.09 mV, 2.01 mV, and 3.84 mV, corresponding to the ΔT of 23 °C, 28 °C, 33 °C, and 38 °C, respectively. The measured U_{oc}s are basically consistent with the results that were calculated using the Seebeck effect.

The output power P is calculated using the following equation [44]:

$$P = I^2 R_{load} = \left(\frac{U_{oc}}{R_{in} + R_{load}}\right)^2 R_{load} \quad (1)$$

where I, R_{load}, and R_{in} are output current, the external resistance, and the internal resistance, respectively. In addition, the power density (P_D) is calculated using the following equation [44]:

$$P_D = \frac{P_{max}}{N \cdot A} = \frac{P_{max}}{N \cdot w \cdot t} \quad (2)$$

where N, A, w, and t are the number of the legs, the cross-sectional area of the leg, the width of the leg, and the thickness of the thin film, respectively. As shown in Fig. 3(f), the output power has the highest value of 3.31 nW when the output current was 1.84 μA under the temperature difference of 38 °C. When the ΔT was 23 °C, 28 °C, 33 °C and 38 °C, the calculated maximum P_D value was 56.14 mWm^{-2}, 75.43 mWm^{-2}, 226.32 mWm^{-2}, and 580.70 mWm^{-2}, respectively. The maximum P_D value is comparable with that of some previous reports [45–47].

4. Conclusions

In this work, flexible Cu_2Se thin films with various atomic ratios were prepared by using a simple layer-by-layer combination reaction method. The self-assembled growth of single α-phase Cu_2Se thin films is successfully realized after annealing. Although the electrical conductivity decreases with an increase in Cu content, a significant increase in the Seebeck coefficient is observed owing to the decrease in carrier concentration. It is observed that the Cu-excess thin films exhibit low thermal conductivity, which is attributed to the nanoplate-like structure and ultimately high ZT value of 0.35, with well-flexible Cu_2Se thin films achieved at room temperature. In addition, the prepared thin film exhibits good flexibility, with about 97% of the original electrical conductivity retention after 800 bending cycles, and the fabricated device has stable output power, with the maximum power density of 580.70 mWm^{-2}. Therefore, the competitive performance of the devices reported in this work has the potential for portable/wearable electronic applications in the field of TE devices.

Credit Author Statement

Xiao-lan Huang: Methodology, Data curation, Investigation. **Dong-wei Ao:** Investigation, Writing- Original draft preparation. **Tian-bao Chen:** Visualization, Investigation. **Yue-xing Chen:** Formal analysis. **Fu Li:** Resources. **Shuo Chen:** Validation. **Guang-xing Liang:** Formal analysis, Resources. **Xiang-hua Zhang:** Writing- Reviewing and Editing. **Zhuang-hao Zheng:** Conceptualization, Supervision, Writing - Review & Editing. **Ping Fan:** Supervision.

Declaration of competing interest

The authors declare that they have no known competing financial interests or personal relationships that could have appeared to influence the work reported in this paper.

Acknowledgments

X.-l.H. and D.-w.A. contributed equally. This work was supported by the National Natural Science Foundation of China (Grant No. 11604212), Guangdong Basic and Applied Basic Research Foundation (2020A1515010515), Shenzhen Key Lab Fund (ZDSYS 20170228105421966), the European Union through the European Regional Development Fund (ERDF), the Ministry of Higher Education and Research, the French region of Brittany and Rennes Metropole. The authors are also thankful for the assistance on STEM-HAADF observation received from the Electron Microscope Center of Shenzhen University.

Appendix A. Supplementary data

Supplementary data to this article can be found online at https://doi.org/10.1016/j.mtener.2021.100743.

References

[1] P.F. Qiu, X. Shi, L.D. Chen, Cu-based thermoelectric materials, Energy Storage Mater 3 (2016) 8.
[2] J. He, T.M. Tritt, Advances in thermoelectric materials research: looking back and moving forward, Science 357 (2017) 6358.
[3] M. Zebarjadi, K. Esfarjani, M.S. Dresselhaus, Z.F. Ren, G. Chen, Perspectives on thermoelectrics: from fundamentals to device applications, Energy Environ. Sci. 5 (2012) 5147.
[4] W.D. Liu, Y. Yu, M. Dargusch, Q. Liu, Z.G. Chen, Carbon allotrope hybrids advance thermoelectric development and applications, Renew. Sustain. Energy Rev. 414 (2021) 110800.
[5] Z.H. Zheng, X.L. Shi, D.W. Ao, W.D. Liu, Y.X. Chen, F. Li, S. Chen, X.Q. Tian, X.R. Li, J.Y. Duan, H.L. Ma, X.H. Zhang, G.X. Liang, P. Fan, Z.G. Chen, Rational band engineering and structural manipulations inducing high thermoelectric performance in n-type $CoSb_3$ thin films, Nano Energy 81 (2021) 105683.
[6] X.L. Shi, W.Y. Chen, T. Zhang, J. Zou, Z.G. Chen, Fiber-based thermoelectrics for solid, portable, and wearable electronics, Energy Environ. Sci. 14 (2021) 729.
[7] L. Wang, Z. Zhang, Y. Liu, B. Wang, L. Fang, J. Qiu, K. Zhang, S. Wang, Exceptional thermoelectric properties of flexible organic-inorganic hybrids with monodispersed and periodic nanophase, Nat. Commun. 9 (2018) 3817.
[8] W. Zhou, Q. Fan, Q. Zhang, L. Cai, K. Li, X. Gu, F. Yang, N. Zhang, Y. Wang, H. Liu, W. Zhou, S. Xie, High-performance and compact-designed flexible thermoelectric modules enabled by a reticulate carbon nanotube architecture, Nat. Commun. 8 (2017) 14886.
[9] S. Huang, Y. Liu, Y. Zhao, Z. Ren, C.F. Guo, Flexible electronics: stretchable electrodes and their future, Adv. Funct. Mater. 29 (2018) 1805924.
[10] S.W. Finefrock, X.Q. Zhu, Y.M. Suna, Y. Wu, Flexible prototype thermoelectric devices based on Ag_2Te and PEDOT:PSS coated nylon fibre, Nanoscale 7 (2015) 5598.
[11] E.W. Zaia, A. Sahu, P. Zhou, M.P. Gordon, J.D. Forster, S. Aloni, Y.S. Liu, J.H. Guo, J.J. Urban, Carrier scattering at alloy nanointerfaces enhances power factor in PEDOT:PSS hybrid thermoelectrics, Nano Lett. 16 (2016) 3352.
[12] C.L. Wan, X.K. Gu, F. Dang, T. Itoh, Y.F. Wang, H. Sasaki, M. Kondo, K. Koga, K. Yabuki, G.J. Snyder, R. Yang, K. Koumoto, Flexible n-type thermoelectric materials by organic intercalation of layered transition metal dichalcogenide TiS_2, Nat. Mater. 14 (2015) 622.
[13] Y. Peng, S.J. Zhu, H.J. Lai, J. Gao, M. Kurosawa, O. Nakatsuka, S. Tanemura, B. Peng, L. Miao, No external load measurement strategy for micro thermoelectric generator based on high-performance $Si_{1-x-y}Ge_xSn_y$ film, J. Materiomics (2020), https://doi.org/10.1016/j.jmat.2020.12.002.
[14] Y. Peng, H.J. Lai, C.Y. Liu, J. Gao, M. Kurosawa, O. Nakatsuka, T. Takeuchi, S. Zaima, S. Tanemura, L. Miao, Realizing high thermoelectric performance in p-type $Si_{1-x-y}Ge_xSn_y$ thin films at ambient temperature by Sn modulation doping, Appl. Phys. Lett. 117 (2020), 053903.
[15] W.Y. Zhao, S.F. Fan, N. Xiao, D.Y. Liu, Y.Y. Tay, C. Yu, D.H. Sim, H.H. Hng, Q.C. Zhang, F. Boey, J. Ma, X.B. Zhao, H. Zhang, Q.Y. Yan, Flexible carbon nanotube papers with improved thermoelectric properties, Energy Environ. Sci. 5 (2012) 5364.
[16] Z. Fan, D. Du, X. Guan, J. Ouyang, Polymer films with ultrahigh thermoelectric properties arising from significant seebeck coefficient enhancement by ion accumulation on surface, Nano Energy 51 (2018) 481.
[17] Q. Jin, W. Shi, Y. Zhao, J. Qiao, J. Qiu, C. Sun, H. Lei, K. Tai, X. Jiang, Cellulose fiber-based hierarchical porous bismuth telluride for high-performance flexible and tailorable thermoelectrics, ACS Appl. Mater. Interfaces 10 (2018) 1743.
[18] Z.Y. Huang, H. Zhang, L. Yang, B. Zhu, K. Zheng, M. Hong, Y. Yu, F.Q. Zu, J. Zou, Z.G. Chen, Achieving high thermoelectric performance of Ni/Cu modified $Bi_{0.5}Sb_{1.5}Te_3$ composites by a facile electroless plating, Mater. Today Energy 9 (2018) 383.
[19] J. Gao, L. Miao, C. Liu, X. Wang, Y. Peng, X. Wei, J. Zhou, Y. Chen, R. Hashimoto, T. Asaka, K. Koumoto, A novel glass-fiber-aided cold-press method for fabrication of n-type Ag_2Te nanowires thermoelectric film on flexible copy-paper substrate, J. Mater. Chem. 5 (2017) 24740.
[20] J. Gao, L. Miao, H. Lai, S. Zhu, Y. Peng, X. Wang, Thermoelectric flexible silver selenide films: compositional and length optimization, iScience 23 (2020) 100753.

[21] Y.X. Chen, X.L. Shi, Z.H. Zheng, F. Li, W.D. Liu, W.Y. Chen, X.R. Li, G.X. Liang, J.T. Luo, P. Fan, Z.G. Chen, Two-dimensional WSe_2/SnSe p-n junctions secure ultrahigh thermoelectric performance in n-type Pb/I Co-doped polycrystalline SnSe, Mater. Today Phys. 18 (2021) 100306.
[22] J.M. Li, H.W. Ming, C.J. Song, L. Wang, H.X. Xin, Y.J. Gu, J. Zhang, X.Y. Qin, D. Li, Synergetic modulation of power factor and thermal conductivity for Cu_3SbSe_4-based system, Mater. Today Energy 18 (2020) 100491.
[23] L.D. Zhao, S.H. Lo, Y. Zhang, H. Sun, G. Tan, C. Uher, C. Wolverton, V.P. Dravid, M.G. Kanatzidis, Ultralow thermal conductivity and high thermoelectric figure of merit in SnSe crystals, Nature 508 (2014) 373.
[24] P. Fan, X.L. Huang, T.B. Chen, F. Li, Y.X. Chen, B. Jabar, S. Chen, H.L. Ma, G.X. Liang, J.T. Luo, X.H. Zhang, Z.H. Zheng, α-Cu2Se thermoelectric thin films prepared by copper sputtering into selenium precursor layers, Chem. Eng. J. 410 (2021) 128444.
[25] H.L. Liu, X. Shi, F.F. Xu, L.L. Zhang, W.Q. Zhang, L.D. Chen, Q. Li, C. Uher, T. Day, G.J. Snyder, Copper ion liquid-like thermoelectrics, Nat. Mater. 11 (2012) 422.
[26] W.D. Liu, L. Yang, Z.G. Chen, Cu_2Se thermoelectrics: property, methodology, and device, Nano Today 35 (2020) 100938.
[27] Z.Y. Lin, Q.Y. He, A.X. Yin, Y.X. Xu, C. Wang, M.N. Ding, H.C. Cheng, B.J. Papandrea, Y. Huang, X.F. Duan, Cosolvent approach for solution-processable electronic thin films, ACS Nano 9 (2015) 4398.
[28] Z.Y. Lin, C. Hollar, J.S. Kang, A. Yin, Y.L. Wang, H.Y. Shiu, Y. Huang, Y.J. Hu, Y.L. Zhang, X.F. Duan, A solution processable high-performance thermoelectric copper selenide thin film, Adv. Mater. 29 (2017) 1606662.
[29] M.R. Scimeca, F. Yang, E. Zaia, N. Chen, P. Zhao, M.P. Gordon, J.D. Forster, Y.S. Liu, J.H. Guo, J.J. Urban, A. Sahu, Rapid stoichiometry control in Cu_2Se thin films for room-temperature power factor improvement, ACS Appl. Energy Mater. 2 (2019) 1517.
[30] J.D. Forster, J.J. Lynch, N.E. Coates, J. Liu, H. Jang, E. Zaia, M.P. Gordon, M. Szybowski, A. Sahu, D.G. Cahill, J.J. Urban, Solution-processed Cu_2Se nanocrystal films with bulk-like thermoelectric performance, Sci. Rep. 7 (2017) 2765.
[31] M.Q. Yang, Z.W. Shen, X.Q. Liu, W. Wang, Electrodeposition and thermoelectric properties of Cu-Se binary compound films, J. Electron. Mater. 45 (2016) 1974.
[32] Y.H. Lv, J.K. Chen, R.K. Zheng, X. Shi, J.Q. Song, T.S. Zhang, X.M. Li, L.D. Chen, (001)-oriented $Cu_{2-y}Se$ thin films with tunable thermoelectric performances grown by pulsed laser deposition, Ceram. Int. 41 (2015) 7439.
[33] K.S. Urmila, T.N. Asokan, R.R. Philip, V. Ganesan, G.S. Okram, B. Pradeep, Structural, optical, electrical and low temperature thermoelectric properties of degenerate polycrystalline Cu_7Se_4 thin films, Phys. Status Solidi B 251 (2014) 689.
[34] A. Ghosh, C. Kulsi, D. Banerjee, A. Mondal, A. Ghosh, C. Kulsi, D. Banerjee, A. Mondal, Galvanic synthesis of $Cu_{2-x}Se$ thin films and their photocatalytic and thermoelectric properties, Appl. Sur. Sci. 369 (2016) 525.
[35] U. Holzwarth, N. Gibson, The Scherrer equation versus the 'Debye-Scherrer equation', Nat. Nanotechnol. 6 (2011) 534.
[36] L. Zhu, H. Xie, Y. Liu, D. Chen, Mingyang Bian, Wenjun Zheng, Novel ultralong hollow hyperbranched $Cu_{2-x}Se$ with nanosheets hierarchical structure: preparation, formation mechanism and properties, J. Alloys Compd. 802 (2019) 430.
[37] J.A. Perez-Taborda, L. Vera, O. Caballero-Calero, E.O. Lopez, J.J. Romero, D.G. Stroppa, F. Briones, M. Martin-Gonzalez, Pulsed hybrid reactive magnetron sputtering for high ZT Cu_2Se thermoelectric films, Adv. Mater. Technol. 2 (2017) 1700012.
[38] H.L. Liu, X. Yuan, P. Lu, X. Shi, F.F. Xu, Y. He, Y. Tang, S.Q. Bai, W.Q. Zhang, L.D. Chen, Y. Lin, L. Shi, H. Lin, X.Y. Gao, X.M. Zhang, H. Chi, C. Uher, Ultrahigh thermoelectric performance by electron and phonon critical scattering in $Cu_2Se_{1-x}I$, Adv. Mater. 25 (2013) 6607.
[39] A. Ghosh, C. Kulsi, D. Banerjee, A. Mondal, Galvanic synthesis of $Cu_{2-x}Se$ thin films and their photocatalytic and thermoelectric properties, Appl. Surf. Sci. 369 (2016) 525.
[40] L. Yang, Z.G. Chen, G. Han, M. Hong, J. Zou, Impacts of Cu defificiency on the thermoelectric properties of $Cu_{2-x}Se$ nanoplates, Acta Mater. 113 (2016) 140.
[41] X.X. Xiao, W.J. Xie, X.F. Tang, Q.J. Zhang, Phase transition and high temperature thermoelectric properties of copper selenide $Cu_{2-x}Se$ ($0 \leq x \leq 0.25$)*, Chin. Phys. B 20 (2011), 087201.
[42] W.W. Liao, L. Yang, J. Chen, D.L. Zhou, X.L. Qu, K. Zheng, G. Han, J.B. Zhou, M. Hong, Z.G. Chen, Realizing Bi-doped α-Cu_2Se as a promising near-room-temperature thermoelectric material, Chem. Eng. J. 371 (2019) 593.
[43] H.L. Liu, X. Yuan, P. Lu, X. Shi, F.F. Xu, Y. He, Y. Tang, S.Q. Bai, W.Q. Zhang, L.D. Chen, Y. Lin, L. Shi, H. Lin, X.Y. Gao, X.M. Zhang, H. Chi, C. Uher, Ultrahigh thermoelectric performance by electron and phonon critical scattering in $Cu_2Se_{1-x}I$, Adv. Mater. 25 (2013) 6607.
[44] J. Choi, J.Y. Lee, S. Lee, C.R. Park, H. Kim, High-performance thermoelectric paper based on double carrier-filtering processes at nanowire heterojunctions, Adv. Energy Mater. 6 (2016) 1502181.
[45] Y. Lu, Y.F. Ding, Y. Qiu, K.F. Cai, Q. Yao, H.J. Song, L. Tong, J.Q. He, L.D. Chen, Good performance and flexible PEDOT:PSS/Cu_2Se nanowire thermoelectric composite films, ACS Appl. Mater. Interfaces 11 (2019) 12819.
[46] Y.F. Ding, Y. Qiu, K.F. Cai, Q. Yao, S. Chen, L.D. Chen, J.Q. He, High performance n-type Ag_2Se film on nylon membrane for flexible thermoelectric power generator, Nat. Commun. 10 (2019) 841.
[47] H.J. Shang, T.G. Li, D. Luo, L. Yu, Q. Zou, D.X. Huang, L.Y. Xiao, H.W. Gu, Z.F. Ren, F.Z. Ding, High-performance Ag-modified $Bi_{0.5}Sb_{1.5}Te_3$ films for the flexible thermoelectric generator, ACS Appl. Mater. Interfaces 12 (2020) 7358.